Goushegir, S.M.; dos Santos, J.F.; Amancio-Filho, S.T.:

Influence of aluminum surface pre-treatments on the bonding mechanisms and mechanical performance of metal-composite single-lap joints

In: Welding in the world (2017) Springer

DOI: 10.1007/s40194-017-0509-y

Influence of aluminum surface pre-treatments on the bonding mechanisms and mechanical performance of metal-composite single lap joints

S.M. Goushegir[a], J.F. dos Santos[a], S.T. Amancio-Filho[a,b,*]

[a] Helmholtz-Zentrum Geesthacht, Centre for Materials and Coastal Research, Institute of Materials Research, Materials Mechanics, Solid State Joining Processes, Max-Planck-Str. 1, 21502, Geesthacht, Germany

[b] Hamburg University of Technology, Institute of Polymer Composites, Denicke Str. 15, 21073, Hamburg, Germany

*Corresponding author. Tel.: +49 4152 87-2066 / -2033
E-mail addresses: mohammad.goushegir@hzg.de, jorge.dos.santos@hzg.de, sergio.amancio@tuhh.de

Abstract

The use of frictional heat for joining thermoplastic-based materials to metals has grown in importance in recent years. Friction spot joining is a relatively new joining technology suitable to join metal-polymer and composite overlap structures. In this work, the influence of various aluminum surface pre-treatments on the bonding mechanisms and mechanical performance of single-lap shear and cross-tensile joints was studied. Mechanical, chemical and electrochemical pre-treatments were applied to the aluminum surface prior to the joining process. All surface pre-treatments increased the joint strength to some extent, compared with specimens without surface pre-treatments. Some of the treatments (chemical and electrochemical) led to the formation of strong chemical bonding between the aluminum and composite. Phosphoric acid anodizing with additional primer layer showed the best performance in increasing the joint's strength. The reason was the strong bond formation between the primer layer and the matrix of the composite during the joining cycle. Moreover, the morphology and chemical composition of the aluminum after surface pre-treatments were analyzed in detail to study the correlation between bonding mechanisms and the mechanical performance of the joints. Finally, fracture surface of the joints was analyzed optically and by SEM, demonstrating parts of the composite remained attached to the aluminum after failure.

Keywords: Friction spot joining; Aluminum and alloys; Composite materials; Surface preparation; Lap joints; Mechanical properties

1. Introduction

Metal-polymer lightweight structures are nowadays increasingly in demand for a wide range of engineering applications, particularly transportation. This is primarily due to their inherent capacity to reduce the weight of an engineering structure, such as components of an aircraft or car. Joining of dissimilar materials such as metal alloys with polymers or composites presents a great challenge due to their distinct physicochemical properties [1]. Rivet-free metal-composite joining techniques, such as adhesive bonding and direct (adhesive-free) adhesion by external heat sources, have the advantage of further weight saving over various mechanical fastening processes. Particularly, newly developed joining techniques such as injection over molding [2], laser joining [3], induction joining [4] and friction spot joining [5] are attractive due to the absence of any additional component, such as a rivet or adhesive, to join the parts together.

Friction spot joining (FSpJ) is an alternative joining technology for producing metal-composite lap joints, patented by and developed at Helmholtz-Zentrum Geesthacht, Germany [6]. As the name implies, FSpJ belongs to friction-based joining technologies. Different aspects of the joints were investigated and described in our previous publications. The process and its feasibility have been studied and microstructural features of the joints were discussed [5,7]. The process was optimized for different combination of materials, considering the formation and mechanical performance of the spot joints [8,9]. Moreover, the interface of the joints was investigated by x-ray photoelectron spectroscopy (XPS) [10], and the fracture micromechanisms of the hybrid joints were discussed into details [11]. Metal-composite FSp joints possess

interfacial bonding mechanisms similar to those reported for adhesive bonding. Adhesion forces and mechanical interlocking are the primary mechanisms holding the joining parts together [5].

It is well understood from the principles of adhesive bonding that the surface energy of the substrate should be higher or equal to the adhesive to achieve a complete wetting, good adhesion, and therefore increased mechanical performance [12-14]. One of the methods frequently used to increase the surface energy of the metal is surface pre-treatment [12,15]. It has been reported that a proper surface pre-treatment should result in a clean surface, without any contamination, increased wettability, adequate surface roughness, mechanical stability and hydrolytic stability [16].

Critchlow and Brewis [17] reviewed more than 40 aluminum surface pre-treatments prior to adhesive bonding. Various mechanical and chemical pre-treatments, conversion coatings, and electrochemical pre-treatment methods have been discussed [17]. In addition to the cleaning effect of the mentioned pre-treatments, surface topography and chemical state are also modified, thereby enhancing the adhesion mechanisms. Extensive studies have been conducted to analyze the influence of different aluminum surface pre-treatments on the topography [18-20], chemical composition [21-24], and strength of the adhesively bonded joints [18,25,26].

Despite the importance of metal surface pre-treatments and their influence on the strength of metal-polymer joints, only limited information is available in the literature in the area of welding-based joining technologies for metal-composite hybrid structures [2,4,27]. Because of the similarities in bonding mechanisms between adhesive bonding and FSpJ, various aluminum surface pre-treatments were used in this work to evaluate their influence on the bonding mechanisms and mechanical performance of the FSp joints. Energy dispersive x-ray spectroscopy (EDS) and scanning electron microscopy (SEM) were employed to analyze the effects of pre-treatments on the surface of the aluminum. Furthermore, the mechanical performance of the produced FSp joints was investigated using single-lap shear (SLS) and cross-tensile (CT) specimens. The fracture surface of the joints after failure was also evaluated visually and in details by SEM analysis. The results obtained in this work give a better understanding of the effects of surface pre-treatments on the bonding mechanisms not only for FSpJ but also for other recently developed welding-based techniques such as laser joining, induction joining and ultrasonic welding.

2. Materials and methods

Aluminum alloy 2024-T3 (AA2024-T3) supplied by Constellium, France with the nominal chemical composition (wt%) 0.1 Si, 0.17 Fe, 4.55 Cu, 0.45 Mn, 1.49 Mg, <0.01 Cr, 0.16 Zn, 0.021 Ti and Al balance was used as the metal component. The nominal thickness of the aluminum sheet was 2 mm. The composite part used in this work was a poly(phenylene sulfide) reinforced with 50 vol% carbon fibers (CF-PPS). The composite sheets supplied by TenCate, the Netherlands had a nominal thickness of 2.17 mm consisting of 5 harness-woven quasi-isotropic laminates. The composite consists of 7 plies of carbon fibers in the following sequence: [(0,90)/(±45)]3/(0,90). AA2024-T3 [28] and CF-PPS [29] were selected because of their applications in the aircraft industry.

2.1. Aluminum surface pre-treatments

To investigate the influence of aluminum surface topography and chemistry on the mechanical performance of the joints, various surface pre-treatments were performed on the aluminum prior to the joining process. Table 1 lists the various surface pre-treatments carried out in this work. Details of each surface pre-treatment are explained following the table.

Table 1 Various aluminum surface pre-treatments performed in this work

Category	Surface pre-treatment	Symbol

As-received	(untreated)	AR
Mechanical	Mechanical Grinding	MG
	Sandblasting	SB
Chemical	Acid Pickling (Etching)	AP
	Conversion Coating	CC
Mechanical & Chemical	Sandblasting + Acid Pickling	SB+AP
	Sandblasting + Conversion Coating	SB+CC
electrochemical	Sulfuric Acid Anodizing	SAA
	Phosphoric Acid Anodizing	PAA
	Phosphoric Acid Anodizing + Primer	PAA-P

a) As-received (AR)

The AR aluminum samples, cut into the required dimensions, were slightly wiped with acetone to remove any loose contaminations. These samples were used as a base reference for comparison with the surface pre-treatments. Acetone wiping was performed prior to all other surface pre-treatments as well.

b) Mechanical Grinding (MG)

Some of the samples were mechanically ground manually using sand paper P1200. The specimens were ground in four directions: parallel (0°) to the rolling direction of the aluminum, followed by 90°, +45° and -45°. After grinding the specimens were cleaned by pressurized air and acetone.

c) Sandblasting (SB)

SB was also carried out manually on a number of the specimens. Several trials were performed to find the optimum SB conditions. Corundum (Al_2O_3) with a particle size in the range of 100-150 µm was used as the medium of treatment. The pressure of blasting was set at 6 bar and the duration of SB at 10 s. The distance between the blasting nozzle and the specimens was 25 cm and the angle to the specimens with respect to the nozzle was 45°. Table 2 lists the chemical composition of the corundum used in this work.

Table 2 Chemical composition of the corundum used in this work [30]

Element	Al_2O_3	Na_2O	Fe_2O_3	SiO_2	Rest
Weight%	99.70	0.20	0.02	0.02	0.06

d) Acid Pickling (AP)

AP was performed using a highly concentrated (65%) nitric acid (HNO_3) solution. The specimens were dipped into the concentrated HNO_3 solution for 15 minutes. Afterward the samples were rinsed under tap water and dried.

e) Conversion Coating (CC)

For CC pre-treatment, Alodine® 4850 (kindly provided by Henkel AG & Co., Germany) was used as the chemical solution. The solution is chromium-free, contains primarily hexafluorozirconate (HFZ) [31], which produces a colorless conversion layer. The concentrated solution was diluted according to the recommendations of the producer: 10 ml of the solution was added to 500 ml distilled water while stirring. The pH of the solution was controlled during the treatment to

be stable at 4. The aluminum specimens were then immersed in the diluted solution for 60 s at room temperature. After this immersion time, the samples were rinsed thoroughly with tap water and dried.

f) Sandblasting + Acid Pickling (SB+AP) / Conversion Coating (SB+CC)

A combination of SB and AP or CC was also carried out to investigate the combined effect of both processes. The samples were first given SB followed by AP or CC.

g) Electrochemical pre-treatments

The electrochemical pre-treatments (SAA, PAA, and PAA-P) were selected based on the literature for adhesive bonding. Specimens were prepared following the internal procedures adopted by one of our project partners.

Besides SEM, laser scanning confocal microscopy (LSCM) (VK-9700, Keyence, Japan) was used as a non-contact method to analyze the roughness of the aluminum surfaces after various surface pre-treatments. Average surface roughness parameters were calculated from 5 different samples; six regions were selected on each sample to measure the surface roughness. The average of these 30 measurements (6 areas on 5 samples) was taken as the surface roughness of each specimen. Two parameters were selected to analyze the surface roughness of the specimens: R_a (arithmetic mean value), which shows the average deviation of peaks and valleys from the mean line on the sampling surface, and R_z gives the distance between the highest peak to the lowest valley.

Note that in the case of mechanical treatments (MG and SB) an area of approximately 25.4 x 30 mm (slightly larger than the considered overlap area of 25.4 x 25.4 mm during the joining process) was pre-treated. The rest of the treatments were applied on the entire surface of the aluminum.

2.2. Wettability

The wettability of the aluminum surface after various pre-treatments was characterized by water contact angle measurement using goniometer method. For this purpose, a contact angle analysis system (Kruess DSA 100, Germany) was employed. A 10 µl water droplet was deposited on the surface of the aluminum and the resultant static contact angle was measured. Enough time (approximately 60 s) was given to the droplet to stabilize itself on the surface of the specimen. The contact angle was measured at five different positions on the aluminum surface and the average of the five measurements was reported as the contact angle. A high-resolution camera was used to capture the image of the droplet.

2.3. Chemical composition analyses

EDS coupled with SEM was carried out to obtain chemical information from the bulk of the specimens for the base materials and the fracture surface of the joints. To obtain and analyze the EDS spectra an EDAX TEAM^{TM} software V4.0.2 was used. Both spot and area analysis were used to characterize small features and larger areas respectively. All EDS spectra were taken with a voltage of 10 kV, the spot size of 3, at a working distance of 10 mm. For the non-conductive specimens, gold sputtering was performed prior to EDS experiments. For those specimens, a gold peak is thereby always present in the respective spectra.

2.4. Mechanical performance

SLS specimens of aluminum and composite with dimensions of 100 × 25.4 mm were machined and the joints were produced with an overlap area of 25.4 x 25.4 mm. The produced FSp joints were then loaded, under lap shear tensile loading until failure, according to the ASTM D3163-01 [32] standard using a universal testing machine (Zwick Roell model 1478) with a load capacity of 100 kN. The traverse test speed was 1.27 mm min^{-1} and the test was performed at room temperature. The average ultimate lap shear force (ULSF) of the joints was obtained using five test replicates.

CT joint geometry was also used in this work to evaluate the mechanical performance of FSp joints following the guidelines in the DIN EN ISO 14272 standard [33]. Similar to SLS testing, a universal testing machine (Zwick Roell

model 1478) with a load capacity of 100 kN was used to evaluate the mechanical performance of the CT joints. The traverse test speed was 2 mm min^{-1} and the tests were performed at room temperature. Three replicates were used to obtain the average ultimate CT force of the joints. The dimensions of the aluminum and composite specimens were 150 × 50 mm with an overlap of 50 × 50 mm. During CT testing, the aluminum was fixed and the load was applied to the composite part of the joint.

Note that in this paper the strength of the joints was referred to the ultimate lap shear force (ULSF) and ultimate cross-tensile force.

2.5. Microscopy analyses

In order to characterize features of the aluminum surface after various surface pre-treatments, and to analyze the joint fracture surfaces SEM (QuantaTM FEG 650 equipment) was used. In the case of aluminum surface analysis, a voltage of 10 kV, the spot size of 3 and a working distance of 10 mm were used. For fracture surfaces, a voltage of 5 kV, the spot size of 3 and a working distance of 15 mm were set. Before analyzing non-conductive samples (e.g., all the fracture surfaces) their surfaces were gold sputtered using a Q150R ES equipment (Quorum Technologies Ltd., England) for 30 s with a current of 65 mA. A very thin layer of gold (a few nm in thickness) makes the samples conductive and facilitates their imaging without hiding any small features of their surfaces.

2.6. FSpJ process

FSpJ was employed to join the parts together using a displacement-controlled machine (RPS100, Harms&Wende, Germany). The principles of the FSpJ process were thoroughly described in our previous publications [5,7-9]. Briefly, a three-pieces non-consumable tool composed of a rotating pin and sleeve, and a stationary clamping ring (Figure 1 (a)) is driven into the upper part (in this case the aluminum sheet) with a pre-defined rotational speed. Frictional heat is generated as a result of the friction between the plunging tool and the aluminum, leading to local plasticization of the aluminum in a volume around the plunging tool (Figure 1 (b) and (c)). As a result of the aluminum softening and the exerted axial force by the tool, the aluminum at the interface with composite locally deforms into an undercut shape (Figure 1 (d)), known as the metallic nub. The slight insertion of the metallic nub into the underlying composite sheet generates mechanical interlocking between the joining partners. Figure 2 demonstrates a sound FSp joint as well as its cross-section in the middle of the spot, indicating the formation of the metallic nub.

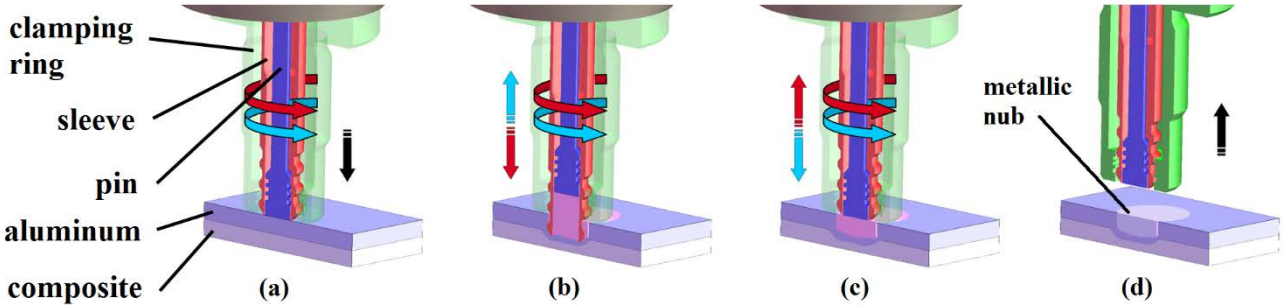

Fig. 1 FSpJ process steps. (a) Tool approaches aluminum sheet, (b) sleeve plunges into the aluminum, (c) sleeve retracts from the aluminum and pin pushes the entrapped metal to the original position and (d) tool retracts and the joint consolidates

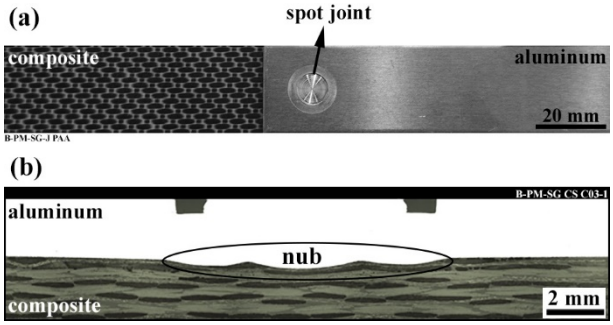

Fig. 2 (a) Top view of a sound FSp join after consolidation and (b) a typical cross-section of an aluminum-composite FSp joint indicating the metallic nub

Moreover, the frictional heat is conducted from the aluminum to the interface with composite. Since the composite possesses low thermal conductivity, the heat mainly accumulates at the interface, leading to the local increase of temperature. Thereby, a thin layer of the matrix of the composite is molten and spreads over the binding area. Adhesion forces are therefore generated between the aluminum and the molten layer after joint consolidation.

The FSpJ process was optimized for the selected base materials in a previous work [9] by statistical analysis. The obtained set of optimized joining parameters which was also used in this work follows: tool rotational speed of 2900 rpm, tool plunge depth of 0.8 mm, total joining time of 4 s and joining pressure of 3 bar.

3. Results and discussion

To explain the mechanical performance of pre-treated AA2024-T3 / CF-PPS FSp joints, the effects of pre-treatment on the surface features of the aluminum are first addressed. To compare the performance of the selected aluminum surface pre-treatments, the optimized set of joining parameters was used. As only one set of joining parameters was investigated, the formation of the nub was similar in all cases and hence the macro-mechanical interlocking was too.

3.1. Aluminum surface analysis

Mechanical interlocking and adhesion forces are the primary bonding mechanisms found in FSpJ. So any alteration on the surface of the aluminum (surface morphology and chemistry) will influence the bonding mechanisms and hence the strength of the FSp joints. Accordingly, it is of utmost importance to examine and understand the aluminum surface modifications as a result of the surface pre-treatments.

3.1.1. Wettability

Water contact angle measurement was used to evaluate the wettability of the aluminum surface after the pre-treatments. Good wettability is an important pre-requisite for achieving good adhesion between a flowing polymer (such as adhesive or the softened composite matrix in FSpJ) and a substrate [34,35]. Table 3 summarizes the results obtained from static

contact angle measurements. One can observe from this table that all the surface pre-treatments used decreased the water contact angle compared to the as-received (AR) specimens. Among all the pre-treatments tested, chemical and electrochemical pre-treatments proved more efficient than mechanical pre-treatments. A reduction in the water contact angle can be attributed primarily to the removal of the contaminations and the natural aluminum oxide (Al_2O_3) from the aluminum surface [36]. To improve the adhesion between the molten PPS composite matrix and the aluminum, obtaining a surface with less contamination plays an important role. High surface energy as a result of reduced contamination enhances the adhesion forces between the PPS and the aluminum.

Table 3 Water contact angle measurements and an example of the water droplet on the AA2024-T3 surface after various pre-treatments

Surface pre-treatment	Contact angle [degrees]	Example of the water droplet on the surface
AR	79 ± 2	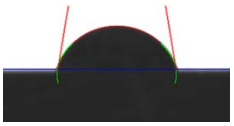
MG	50 ± 2	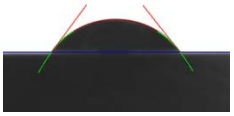
SB	35 ± 2	
Chemical and electrochemical pre-treatments, as well as mechanical + chemical pre-treatments	< 5	No image could be obtained as a result of very low contact angle and instability of the water droplet

In addition to the cleaning effect of the surface pre-treatments used in this work, the positive effects of increased surface roughness were observed, particularly resulting from mechanical pre-treatments. As Wenzel argues [37], increased effective surface area due to the generation of macro-rough and micro-rough asperities improves the wettability of the aluminum surface. Sandblasting proved an effective pre-treatment, producing a very macro-rough surface, which indeed led to an effectively large surface area on the aluminum and so improved wettability. Although, the effectiveness of mechanical grinding (MG) was not as much as SB to improve the wetting of the surface, it reduced the contact angle by approximately 30° compared to the AR samples. This is due to the larger effective surface area, compared to the AR specimen. Chemical and electrochemical pre-treatments resulted in a surface with highly micro-rough asperities, which reduced the contact angle enormously, to below 5°. Aspects of aluminum surface morphology will be further discussed later.

Physicochemical alteration of the surface is another issue that should be taken into account. Surface energy is also changed as a result of modifications to the surface composition. Even mechanical pre-treatments, such as sandblasting,

may alter the surface energy as a result of varying the chemical composition (depending on the medium used for the pre-treatment), as reported by Harris and Beevers [18].

3.1.2. Surface topography and morphology

Obtaining a rough surface, to a certain extent, was one of the primary motivations to employ various surface pre-treatments. In particular, the aim was to achieve a macro-rough surface as a result of mechanical pre-treatments and a micro-rough surface through the application of the chemical and electrochemical pre-treatments. Table 4 lists the average surface roughness parameters (R_a and R_z) of the AA2024-T3 after applying each surface pre-treatment. It is apparent from the table that both MG and SB successfully increased the aluminum surface roughness compared to the AR state, and the increase was much higher using SB. Obviously, excessive surface roughness is detrimental to the mechanical performance because larger asperities can act as barriers to the molten polymer flow, reducing the wettability [18] and the bonding area. Despite this, such a negative effect was not detected in this work. SB generated a macro-porous aluminum surface that effectively increased the micromechanical interlocking. In particular, very large R_z shows the ability of the SB specimens to accommodate a large amount of molten PPS. Chemical pre-treatments did not show any influence on the R_a, although they did increase R_z and that can slightly contribute to an increase in mechanical interlocking. It is interesting that CC pre-treatment produced the same surface roughness as AP pre-treatment, but much faster (1 min as opposed to 15 min of pre-treatment respectively). This may be related to the effectiveness of the fluoride ions in the CC solution in rapidly attacking the aluminum surface [21]. A combination of mechanical (SB) and chemical pre-treatments also resulted in a large surface roughness. However, the values of R_a and R_z were reduced, compared to the stand-alone SB. This is in fact due to partial removal of surface ridges by the chemical etching.

Electrochemical pre-treatments produced similar surface roughness to chemical pre-treatments. It should be noted that in cases of chemical and electrochemical pre-treatments a very fine microporous oxide layer is expected to be formed. It seems that in such cases the effectiveness of surface roughness analysis is questionable.

Table 4 Average surface roughness parameters of the AA2024-T3 after various surface pre-treatments obtained by non-contact LSCM

Category	Surface pre-treatment	R_a [µm]	R_z [µm]
As-received	AR	0.4	16.9
Mechanical	MG	0.7	30.1
	SB	5.2	100.1
Chemical	AP	0.4	32.8
	CC	0.4	32.7
Mechanical & Chemical	SB+AP	3.9	69.4
	SB+CC	3.9	75.8
Electrochemical	SAA	0.8	38.2
	PAA	0.6	38.8
	PAA-P	1.1	21

SEM was used to examine the morphology of the oxide layer on the aluminum surface. As can be observed in Figure 3 (a), the AR specimens showed a smooth, featureless surface. Only some rolling lines are visible on the surface. The smoothness of their surfaces was confirmed by the results of surface roughness analysis presented in Table 4. Unlike the AR specimens, the mechanically ground samples had slightly rough, parallel lines from the final stages of manual grinding in one direction, as shown in Figure 3 (b). The generated groove-like features and some other irregularities on the surface led to a slightly higher surface roughness, as shown in Table 4. However, markedly more modification by mechanical pre-treatment was identified on the SB surfaces. As illustrated in Figure 3 (c), with SB a very rough surface with different irregular shapes was obtained. The molten PPS layer can readily penetrate into porosities and crevices leading to a strong micromechanical interlocking effect. As explained by Packham [38], the shape and angle of surface asperities play an important role in mechanical interlocking between a polymer (such as an adhesive) and a substrate, which in turn influences the mechanical performance of a joint. It is believed that as SB generated asperities with various shapes and angles it can effectively increase micromechanical interlocking, both under shear and normal loading. Furthermore, the larger effective surface area obtained by SB increases the contact between PPS and the aluminum, leading to the promotion of adhesion forces across an extended area.

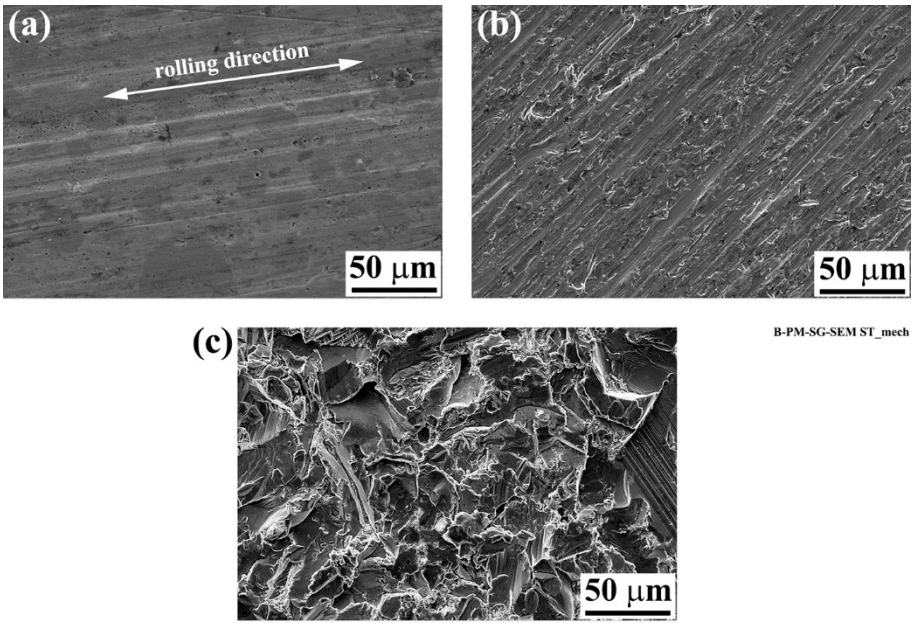

Fig. 3 SEM images of the AA2024-T3 surface from (a) as-received (AR), and after (b) mechanical grinding (MG) and (c) sandblasting (SB) pre-treatments

The surface features of the chemically pre-treated aluminum are shown in Figure 4. Both AP and CC pre-treatments led to surfaces very similar to the AR surface. No specific features could be identified apart from some slight scratches and localized etch pits. The rolling lines were also retained to some extent after both pre-treatments. Chemical conversion treatments, for example Ti/Zr, usually lead to the formation of a uniform layer consisting of spherical particles [21,24]. In the current work, we did not detect such a layer on the surface of the CC pre-treated aluminum. This could be due to differing chemical compositions of CC solutions and to the duration of the treatment being shorter in this study. The influence of parameters such as duration of pre-treatment, the concentration of the solution, etc. on the formation and morphology of the CC layer was not considered.

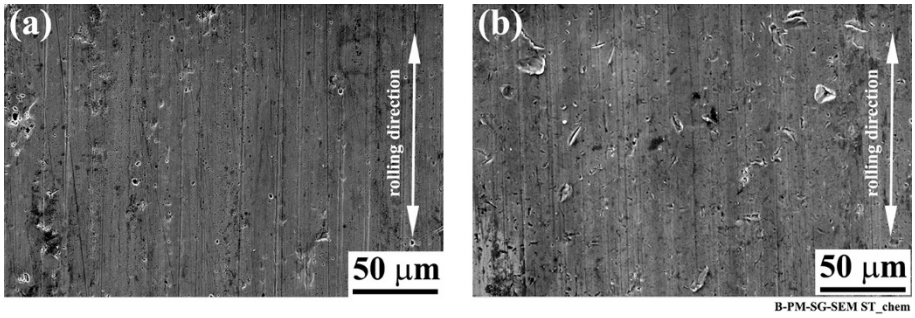

Fig. 4 SEM images of the AA2024-T3 surface after (a) acid pickling (AP) and (b) conversion coating (CC) pre-treatments

Figure 5 illustrates the aluminum surface features after electrochemical pre-treatments. The SAA pre-treated surface (Figure 5 (a)) demonstrated a combination of aspects. Firstly, the surface showed an incomplete coverage, which most probably occurs at the grain boundaries. Such a structure was observed by Lunder *et al.* [39] in the chromate conversion coating of AA6060, and a similar feature was also found by Critchlow *et al.* [16] in the chromic acid anodizing of AA2024-T3 clad. Secondly, very few scalloped features could be identified, similar to [16,39]. In addition, a few shallow rolling lines were still observed on the surface. The presence of these features can increase the micromechanical interlocking between the molten PPS and the oxide layer, leading to an increase in the strength of the joints.

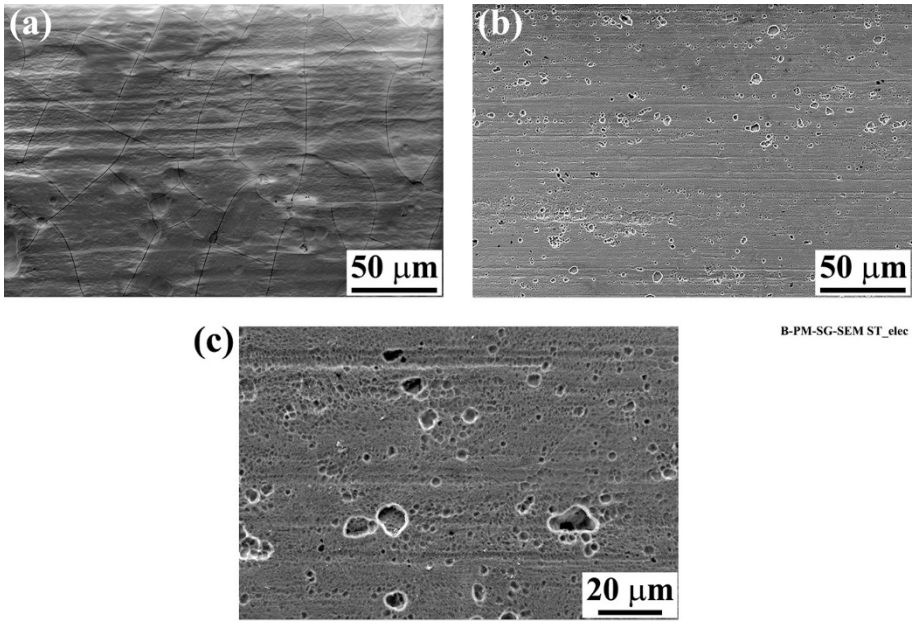

Fig. 5 SEM images of the AA2024-T3 surface after (a) sulfuric acid anodizing (SAA) and (b) phosphoric acid anodizing (PAA) pre-treatments, and (c) high magnification image of the PAA pre-treated surface

At low magnification (Figure 5 (b)) the PAA pre-treated specimens showed a porous surface with relatively small generated pores. A higher magnification image of the surface (Figure 5 (c)) revealed a very porous oxide layer, similar to those reported in the literature [40-43]. A few larger pores were also detected on the surface. Such very fine porous structure promotes the micromechanical interlocking phenomenon and is believed to increase the strength of the joint. It was reported [40] that such a fine porous structure is responsible for achieving strong joints in adhesive bonding as well. It is, however, important to mention that, in contrast to the adhesive bonding, for the current FSp joints a very fine porous structure may not prove so beneficial. Due to the fact that PPS is in a molten or softened state only for a few seconds, there may not be enough time for it to complete the pore penetration and result in effective micromechanical

interlocking. This aspect of completing the pore filling is especially important for achieving a durable joint, as discussed by Digby and Packham [44].

Figure 6 shows a low magnification SEM image of the surface of the aluminum after PAA pre-treatment and the subsequent application of primer. The surface illustrated has a very dense and compact structure with very small and elongated whisker-like particles deposited homogeneously on the surface. These particles were examined by means of EDS, which showed the presence of strontium oxide and chromium oxide. The chemical composition of the aluminum surface will be discussed next.

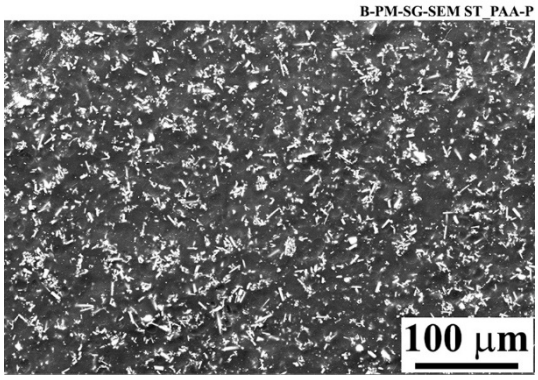

Fig. 6 SEM image of the AA2024-T3 surface after phosphoric acid anodizing + primer (PAA-P) pre-treatment

3.1.3. Surface chemical composition

In addition to the topography and morphology of the surface, which affect micromechanical interlocking, alteration of the chemical composition as a result of surface pre-treatments influences the adhesion forces between the PPS and AA2024-T3. Therefore, the surface chemical composition of the aluminum was also investigated, using EDS and XPS.

Figure 7 illustrates the EDS spectra of the aluminum surface in the AR condition and after the various surface pre-treatments. As examples here, the spectrum of only one treated sample in each category of surface pre-treatments (see Table 1) is shown in this figure. The average surface chemical composition of all the surface pre-treated specimens obtained from the EDS analysis is however tabulated in Table 5. The spectra selected were for those specimens with highest mechanical performance in each category (which will be explained in the next section). It is clearly visible that apart from the PAA-P specimens the amount of surface carbon is reduced by all other surface pre-treatments, compared to the AR condition. This is one of the reasons why the wettability of the aluminum surface was increased and the water contact angle reduced (see Table 3). Organic contaminations may adhere to the aluminum due to the aluminum sheet processing or during the machining of the coupon specimens. Such contaminations are not easily eliminated by a simple wiping procedure (in AR condition) and often require a stronger surface cleaning such as chemical treatments. In addition, the PAA-P specimens showed a high amount of carbon on the surface, confirming the presence of a thick layer of the epoxy-based polymeric primer.

In all surface pre-treated specimens, the amount of Cu and Mg was also reduced, compared to the AR samples. This is probably due to the removal of secondary particles (typically found in AA2024-T3 [45-47]) by mechanical pre-treatment or dissolution of the particles by chemical and electrochemical pre-treatments. In the PAA-P specimens, no Cu or Mg could be detected due to the deposition of the relatively thick (approximately 7 μm) primer layer. The variation of Al and O was slightly different as a result of surface pre-treatments. It seems that to some extent MG removed the aluminum's natural oxide leading to a higher amount of Al and lower amount of O. By contrast, SB, AP, and CC did not change the composition drastically. It is believed that the oxide layer generated by these surface pre-treatments was not extended or

thickened, compared to the AR condition. Similar behavior was also reported in [48] for mechanical and chemical surface pre-treatments of AA2024.

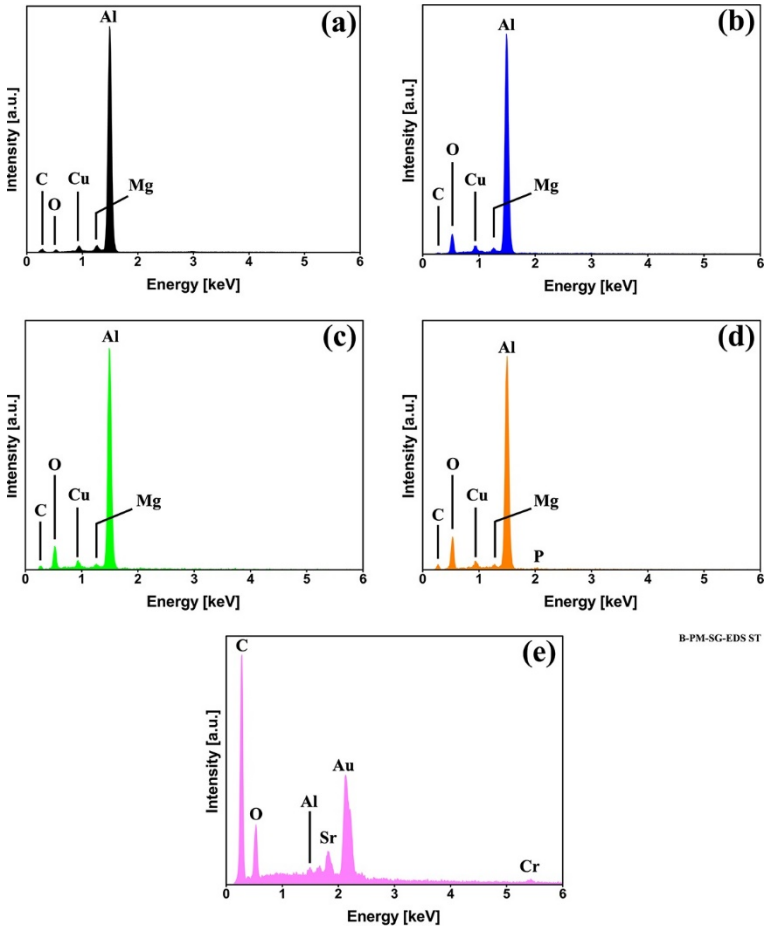

Fig. 7 Example of selected spectra from the EDS analysis of the AA2024-T3 surface; from (a) as-received (AR), (b) sandblasting (SB), (c) conversion coating (CC), (d) phosphoric acid anodizing (PAA), and (e) phosphoric acid anodizing + primer (PAA-P)

However, SAA and PAA pre-treatments showed a high amount of O, implying the formation of a thicker oxide layer on the aluminum surface after the anodizing process. Comparing the amount of O and Al for SAA (O: 49.9%; Al: 38.3%) and for PAA (O: 14.9%; Al: 76.9%) pre-treatments suggests that the oxide layer formed after SAA pre-treatment was much thicker than the PAA one. This agrees with the results published in the literature, as an example in [49]. Nevertheless, another reason for the high amount of O in the SAA specimen could be attributed to absorbed water. It has been explained that the SAA pre-treated aluminum is highly susceptible to water absorption [49,50]. A small amount of sulfur was also detected on the surface of the SAA pre-treated samples due to the anodizing solution, which contained sulfuric acid, and this could be related to the formation of aluminum sulfate [50]. A low concentration of P could also be detected on the surface of the PAA pre-treated aluminum. Phosphorous is reported to form an $AlPO_4$ monolayer on the top surface of aluminum [51-53].

Moreover, the PAA-P specimens showed a very low amount of Al in the spectra obtained. This is due to a thick layer of deposited primer, which masked detection of the bulk aluminum. In addition, a relatively high O content was detected for the PAA-P pre-treated surfaces. The epoxy-based primer contains O in its structure, which is one source of this oxygen. Chromium oxide and strontium oxide are also normally used in the primer layer as corrosion inhibitors [54], which are further sources of oxygen. The presence of Cr and Sr were also confirmed by the EDS analysis as can be seen in Figure 7

(e) and Table 5. Chromium oxide and strontium oxide were identified on the PAA-P pre-treated surfaces as whisker-like particles as illustrated in Figure 6.

Table 5 Average chemical composition (in wt%) of the AA2024-T3 surface after different surface pre-treatments by EDS analysis

Surface pre-treatment	Al	O	C	Cu	Mg	P	S	Cr	Sr
AR	78.4	6.0	6.5	4.9	4.2	-	-	-	-
MG	92.3	1.3	0.4	3.8	2.2	-	-	-	-
SB	87.3	6.8	1.2	3.1	1.6	-	-	-	-
AP	85.5	4.9	3.8	4.1	1.7	-	-	-	-
CC	88.1	5.1	1.5	3.9	1.4	-	-	-	-
SAA	38.3	49.9	2.4	3.1	0.4	-	5.9	-	-
PAA	76.9	14.9	2.0	3.0	1.5	1.7	-	-	-
PAA-P	0.2	17.8	76.0	-	-	-	-	2.5	3.5

The EDS analysis provided useful information on pre-treatment alterations of the chemical composition on the aluminum surface. Such changes in chemical composition and an oxide layer generated on the surface influence the adhesion between the aluminum and PPS and hence the mechanical performance of the joints. However, in some surface pre-treatments, particularly CC, a more fundamental composition alteration was expected, because of the hexafluorozirconate (HFZ) basis of the alodine solution used in this work [31]. As the information depth by EDS was large, chemical information for just the top surface could not be obtained. Therefore, XPS analysis was also performed, to better understand the chemical composition modifications of the aluminum surface. Note that XPS results are presented for those pre-treatments that EDS did not give enough information. These modifications might be occurred on the top surface of the aluminum in the range of nanometers and may not be detected by EDS analysis.

We previously showed [10] by XPS analysis that CC leads to the formation of a thin layer consisting Al-Zr-O-F complex as a result of the interaction between aluminum surface and hexafluorozirconate (HFZ) in the alodine solution. This layer is believed to possess low interfacial tension and to increase the activation and wettability of the aluminum surface [21]. Such increase in wettability and hydrophilicity was observed in this work as also shown in Table 3. The main reaction products of the HFZ solution with the aluminum surface were reported to be zirconium oxide and aluminum fluoride [55,56]. The formation of a complex layer with new elements is thought to increase the possibility of the chemical bond formation between the pre-treated aluminum surface and the molten PPS layer. It was shown that Al-C and C-Zr were the bonds formed at the interface of the aluminum – composite [10]. Similar results were obtained by applying PAA on the surface of the aluminum. XPS interfacial analysis of the PAA pre-treated specimens showed the formation of Al-C bonds at the interface [10]. Such bond formation is supposed to increase the strength of the hybrid joints.

3.2. Mechanical performance of the joints

This section deals with the mechanical performance of the FSp joints and its relation to changes on the aluminum surface. The main mechanical testing used in this work was SLS testing. In addition, CT joint geometry was examined

for selected surface pre-treatments to evaluate the joint behavior and the influence of surface pre-treatments under mode I loading.

Table 6 lists the average strength and displacement at the peak load of the SLS FSp joint with the various surface pre-treatments. All surface pre-treatments increased the SLS strength of the joint compared to the AR specimen (strength 878 ± 89 N). Such an increase was particularly pronounced in the case of the PAA-P pre-treatment.

Table 6 Average strength and displacement at the peak load of the SLS FSp joints after aluminum surface pre-treatments

Surface pre-treatment	Average SLS strength [N]	Standard deviation [N]	Average displacement at the peak load [mm]	Standard deviation [mm]
AR	878	89	0.2	0.0
MG	2352	182	0.7	0.1
SB	2324	151	0.7	0.1
AP	1246	186	0.4	0.1
CC	2493	118	0.8	0.0
SB + AP	3028	228	0.8	0.1
SB + CC	3276	352	0.9	0.1
SAA	2149	75	1.1	0.3
PAA	3276	115	1.4	0.2
PAA-P	8788	62	1.8	0.0

Both MG (strength 2352 ± 182 N) and SB (strength 2324 ± 151 N) specimens showed an increase of more than 150% compared to the AR specimen. As explained previously, both mechanical pre-treatments increased the surface roughness, by introducing parallel grooves in the case of MG or asperities and irregularities with SB. Although SB gave a much rougher surface than MG, their similar mechanical performance, in terms of SLS strength, suggests that the groove-like features produced by MG were sufficient to generate micromechanical interlocking between the molten PPS and aluminum under shear loading. As the final grinding direction was ±45° to the loading direction, efficient interlocking was achieved.

AP had the lowest increase in strength (1246 ± 186 N) of approximately 42%. Since AP does not change the chemistry of the surface, such an increase in strength can be attributed to a slight increase in surface roughness, and so a small increase in micromechanical interlocking. Improved micromechanical interlocking was particularly achieved due to efficient wetting of the aluminum by the molten PPS. CC had a similar surface topography to AP (see Table 4), but the increase in strength (2493 ± 118 N) was over 180%, compared with the AR specimen. In addition to improved wettability, similar to the AP pre-treatment, CC altered the chemical composition markedly. The formation of strong chemical bonds is thought to be the main cause of such an increase in the strength of the CC pre-treated specimen. Zr-C and Al-C were claimed to be the main interfacial bonds formed during FSpJ of the CC-pretreated aluminum and CF-PPS [10]. The formation and nature of interfacial bonds during FSpJ were thoroughly explained in [10]. A combination of SB

with AP and CC further increased the strength of the joint (3028 ± 228 N and 3276 ± 352 N respectively) which was expected. Both micromechanical interlocking and the formation of chemical bonds (in the case of the SB+CC pre-treatment) in addition to improved wettability are the main reasons for such improvement.

Electrochemical pre-treatments also positively influenced the strength of the joints, but PAA performed better than SAA (3276 ± 115 N and 2149 ± 75 N respectively). As discussed earlier, the SAA pre-treatment led to the formation of a very small number of scalloped features and incomplete coverage at the grain boundaries was also identified (see Figure 5 (a)). The penetration of the molten PPS into these features is believed to increase micromechanical interlocking. In the case of the PAA pre-treatment, the generation of a highly porous oxide layer also improved the micromechanical interlocking. Although the pores were very fine after PAA pre-treatment and the PPS was only a few seconds in the molten state, sufficient pore filling was probably achieved to improve the micromechanical interlocking and increase the strength of the joint under quasi-static loading. The lower strength of SAA pre-treated specimens compared to their PAA counterparts might be related to the hydrated state of the aluminum oxide layer after SAA pre-treatment. It was shown that the aluminum surface after SAA pre-treatments contains up to 15 wt% aluminum sulfate [49,50]. Aluminum sulfate is very susceptible to water absorption and this may lead to a large amount of water absorption if the aluminum is exposed to a humid environment [49,50]. Such hydrated oxide may be detrimental to the joint strength.

Finally, the PAA-P specimen had the highest average strength of 8788 ± 62 N, which is approximately 10 times the AR condition. This prominent increase in strength is believed to result from the formation of primary carbon-carbon chemical bonds between the primer layer and the molten PPS. As surface roughness was not altered markedly after PAA-P pre-treatment, the cause of this strength increase must be mainly due to the promotion of adhesion forces by the formation of chemical bonding. Kinloch *et al.* [57] observed in adhesive bonding of aluminum joints that the primer forms an interphase with the underlying oxide layer. Such an interphase between the oxide layer and the adhesive decreases the local stress concentration between the high-modulus oxide layer and low modulus adhesive [57]. A similar interphase with intermediate modulus may be formed during the FSpJ process, between the aluminum oxide and molten PPS, leading to better crack resistance and hence improved joint strength.

As can be seen in Table 6 the displacement at the peak load follows the same trend as the SLS strength of the joints, with PAA-P showing the highest displacement. However, all the joints demonstrated a linear elastic behavior, with limited displacement, before final catastrophic failure. This behavior is illustrated in Figure 8 as an example for PAA-P specimens. The linear elastic behavior of the FSp joints was described recently in another manuscript [11].

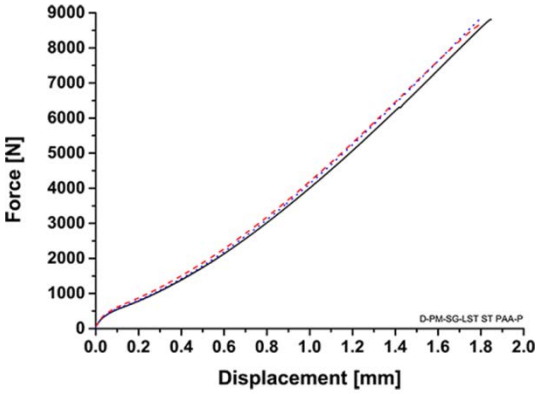

Fig. 8 Force (load) – displacement curves of PAA-P FSp joint under lap-shear loading. The figure shows three test replicates

To understand the effectiveness of surface pre-treatments and joint behavior under mode I tensile loading, CT geometry was selected. Table 7 lists the CT strength (achieved ultimate CT force) and the displacement at the peak load of the FSp joint for selected pre-treatments.

Table 7 Average strength and displacement at the peak load of the cross-tensile FSp joints after aluminum surface pre-treatments

Surface pre-treatment	Average CT strength [N]	Standard deviation [N]	Average displacement at the peak load [mm]	Standard deviation [mm]
MG	253	16	0.5	0.0
SB	507	101	1.0	0.1
CC	497	80	1.3	0.2
SB + CC	585	76	1.5	0.2
PAA	888	41	2.7	0.2
PAA-P	1078	58	2.7	0.1

One observes that the strength of the joint under tensile loading is much lower than under shear loading. CT strength of the FSp joint was approximately 10-30% of the respective SLS strength for the various surface pre-treatments. This is due to the fact that bonding mechanisms in FSpJ, particularly mechanical interlocking as a result of the nub formation and aluminum surface roughness, act more efficient under shear loading. As can be seen in Figure 2 (b), the metallic nub, in the form of an undercut, is slightly inserted into the composite and a part of the molten polymer is accommodated into it. From the shape of the nub, it can be assumed that it is not very effective to strengthen the joint under tensile loading. Moreover, the shape and angle of the surface asperities, schematically shown in Figure 9, play an important role in increasing the strength of the joint [38]. These are more effective under shear loading compared to tensile loading. Asperities of type “a” and “c” can only effectively increase the interlocking effect, and hence the joint’s strength under shear loading. Only irregularities of type “b” (ink-bottle pores) may also contribute to the joint’s strength under mode I tensile loading. From all surface pre-treatments used in this work, only SB and PAA are believed to generate all types of irregularities including type “b”.

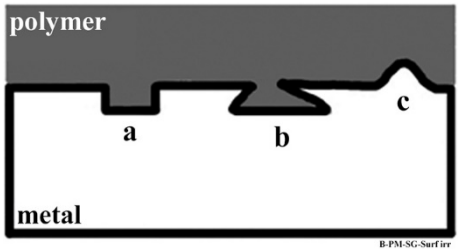

Fig. 9 Schematic illustration of various types of metal surface irregularities in contact with a molten polymer. Adapted from [58]

Comparison of surface pre-treatments reveals that among the mechanical pre-treatments, SB outperformed MG (strength 507 ± 101 N and 253 ± 16 N respectively). Although the groove-like features in the MG specimen were efficient enough to increase micromechanical interlocking under shear loading, they have a reduced performance under tensile loading. However, the irregularities of the SB specimen seem to be sufficient to generate more suitable micromechanical interlocking. The stand-alone CC exhibited a similar strength to the SB specimen (497 ± 80 N), which shows that micromechanical interlocking, as a result of SB, and adhesion forces, due to chemical bonding in the CC specimen, exert similar influences on the mode-I strength of the joint. This behavior was also observed with SLS geometry, as listed in Table 6. Analogous to the behavior of SLS geometry, the SB+CC specimen showed slightly higher cross-tensile strength (585 ± 76 N) than stand-alone SB and CC due to the combined effects of micromechanical interlocking and chemical bonding.

The PAA specimen had an average cross-tensile strength of 888 ± 41 N and that is approximately 77% higher than SB or CC pre-treatments. This is probably due to the shape of the fine pores formed on the aluminum surface after PAA pre-treatment, which also improves the micromechanical interlocking under tensile loading. In order to confirm this hypothesis, advanced analysis is required, such as by transmission electron microscopy (TEM) of the joint cross-section, which was beyond the scope of this work. Similar to the SLS results, PAA-P achieved the highest cross-tensile strength (1078 ± 58 N) among the surface pre-treatments tested, due to the strong primary bonds between the primer layer and PPS.

A similar behavior was also seen with the displacement at the peak load as listed in Table 7. Such behavior was expected (similar to the SLS specimens) because the joints demonstrate a linear elastic trend. Therefore, the higher the joint strength is, the larger the displacement will be. An example of the force – displacement curves corresponding to the PAA-P specimens is shown in Figure 10.

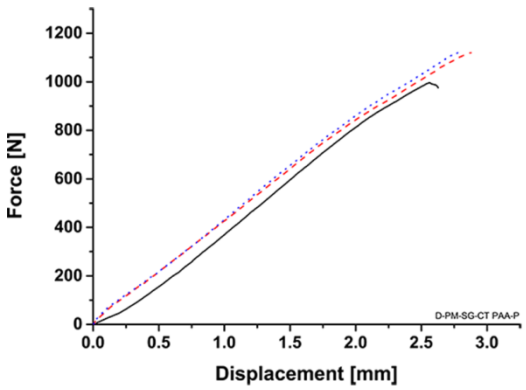

Fig. 10 Force (load) – displacement curves of PAA-P FSp joint under cross-tensile loading. The figure shows three test replicates

Cross-tensile testing has not been used frequently in the literature to evaluate the mechanical performance of metal-polymer joints. From the scarce results in the literature, for example, Seidlitz *et al.* [59] reported on the cross-tensile strength of steel / GFRP riveted joints. CT forces between approximately 500 N and 1200 N were reported in their work. Therefore, the CT strength of the FSp joints obtained in this work gives comparable qualitative results with those reported in [59], despite differences in the employed joining techniques and base materials.

3.3. Failure and fracture surface analysis

In this section, the fracture surfaces from the selected pre-treatment categories are analyzed for the SLS joint geometry. Due to similarities in the failure mechanisms, from each category, the best surface pre-treatment, based on SLS strength, was selected for the analysis. Figure 11 illustrates the overview of the fracture surface of the SB, CC, PAA, and PAA-P pre-treated specimens. Generally, all the fracture surfaces have similar macro features. Similar to our previous explanations in [7] the pre-treated FSp joints also failed under shear mode and frequently in the composite. For SB, CC, and PAA specimens no aluminum residues could be identified on the composite side (neither visually nor through SEM examination), but some of the PPS and carbon fibers remained attached to the aluminum after mechanical testing. Radial cracks initiate at the outer periphery of the PPS molten layer and propagate at the interface between this layer and the composite surface until reaching the center of the joint, following the same pattern as reported in [7,11]. Further, in the central region of the joint, the cracks propagate into the first plies of the CF-PPS leaving parts of the PPS and carbon fibers attached to the aluminum after final failure [7,11]. For more information on the bonding zones, failure and fracture micromechanisms in FSpJ refer to [11]. In the fracture surfaces of the PAA-P specimens (Figure 11 (d)) yellowish features could be detected on the composite surface, as indicated by the white arrows. These features are believed to be primer material removed from the pre-treated aluminum surface. As a result of the strong bonds generated between the primer and PPS, the crack frequently alters its propagation path between within the primer and the molten PPS layer.

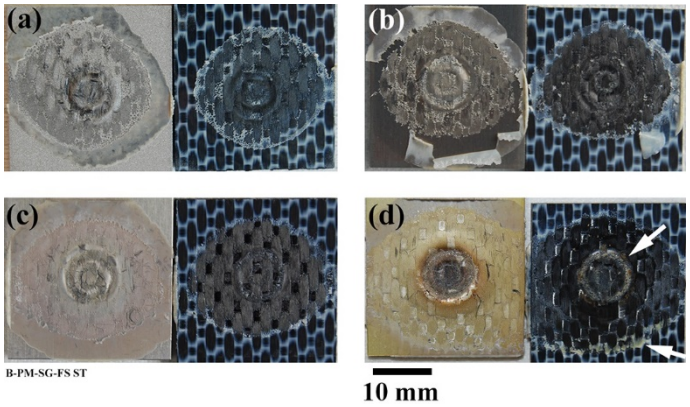

Fig. 11 Fracture surfaces of the SLS joints; (a) sandblasting (SB), (b) conversion coating (CC), (c) phosphoric acid anodizing (PAA), and (d) phosphoric acid anodizing + primer (PAA-P). White arrows in (d) indicate primer remaining attached to the CF-PPS

To further evaluate the yellowish features on the composite, SEM and EDS analysis were employed. Figure 12 shows the SEM images from the composite side in Figure 11 (d) close to the edge of the composite indicated by the lower white arrow. Two parts were detected on the surface of the composite. A high-magnification SEM image of the white rectangle in Figure 12 (a) is shown in Figure 12 (b). Strong bonding between the primer layer and the underlying PPS could be identified because no detachment of the two layers was detected in the SEM images. Moreover, the PPS below the primer layer shows elongated features approximately perpendicular to the loading plane. This could be an indication of out-of-plane forces as a result of the secondary bending effect, particularly near to the edges of the overlap area.

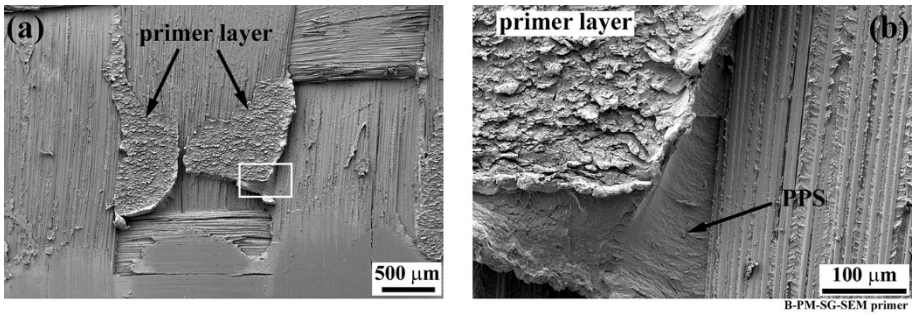

Fig. 12 SEM imaging of the fracture surface of the CF-PPS; (a) primer residues remain attached to the composite, and (b) a high magnification image of the white rectangle in (a)

To further confirm that such layers are in fact removed primer, EDS analysis was performed at a high magnification as shown in Figure 13 (a). Two spots were selected for the analysis as shown in this figure. The EDS spectra of both spots are also illustrated in Figure 13. The spectrum of Spot 1, (Figure 13 (b)), contains several elements in which carbon has the highest concentration of 70 wt%. Although the carbon can be related both to the primer and PPS, the presence of O (11 wt%), Sr (7 wt%), and Cr (6 wt%) reveal that this spot refers to the primer that contains chromium and strontium oxides. Furthermore, a small amount of Al (2 wt%) was also identified in this spectrum, which suggests that the failure in some regions might have occurred in the underlying aluminum oxide. This is an indication of very strong bonding between the primer and the aluminum oxide. A small amount of S (4 wt%) was also detected, which is due to failure of the composite part (PPS matrix). By contrast, the spectrum of Spot 2 (Figure 13 (c)) reveals only 3 elements; C (62 wt%), S (34 wt%), and Cr (4 wt%). This indicates that this spot relates to a PPS-rich area. EDS analysis of the CF-PPS showed a carbon content of approximately 55 wt% and sulfur 45 wt%. Therefore, the higher C ratio in Spot 2 suggests that the

primer is another source of the carbon in this position. In addition, the small amount of Cr in Spot 2 also originated from the whisker-like particles in the primer.

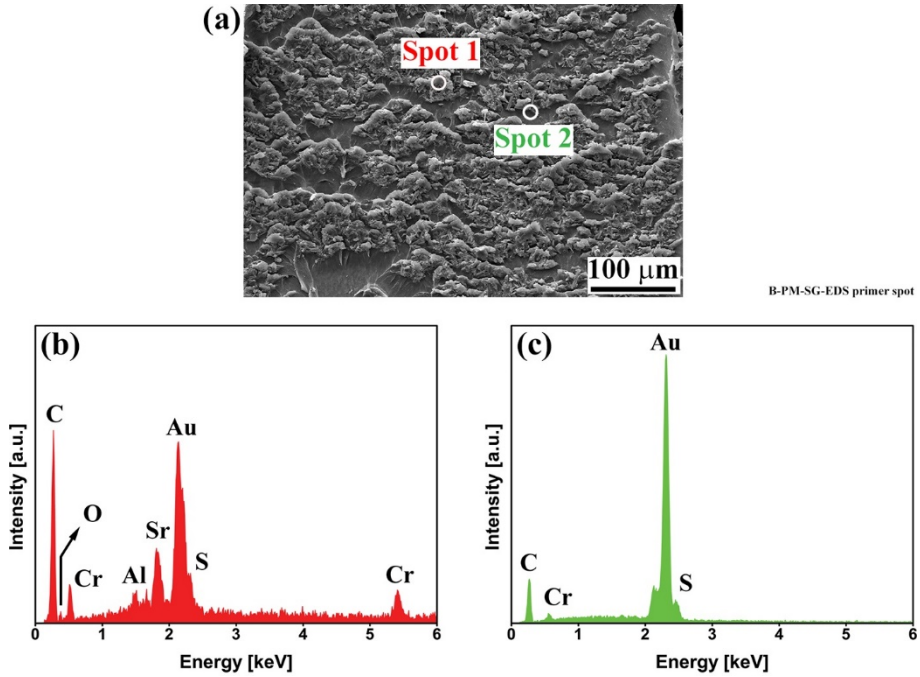

Fig. 13 (a) SEM image of the primer layer remained attached to the composite, (b) EDS spectrum of Spot 1 in (a), and (c) EDS spectrum of Spot 2 in (a)

In summary, in all surface pre-treated specimens except PAA-P, the failure in the center of the joint takes place inside the composite because a layer of the PPS could be identified on the aluminum side. However, for the PAA-P specimens, the failure occurs both in the PPS and the primer, where the crack alters its path frequently between the two. In some places, the crack may further propagate into the aluminum oxide beneath the primer layer.

4. Conclusions

Various aluminum surface pre-treatments were used in this work to investigate their influence on the bonding mechanisms and mechanical performance of FSp joints. Removal of surface contaminations, generation of macro-rough and micro-rough asperities, and alteration of the surface chemical composition led to enhancement of the surface energy and improved wettability of the surface of the AA2024-T3. The following conclusions could be drawn from this work:

- Mechanical pre-treatments, especially sandblasting, drastically increased the average arithmetic surface roughness (5.2 microns in comparison to AR with 0.4 microns), however, noticeable changes in chemical composition could not be detected.
- Acid pickling and conversion coating led to a clean surface with a low amount of contaminations, but the average surface roughness did not alter (0.4 microns similar to AR surface). Unlike acid pickling, which did not reveal any changes in the chemical composition of the surface, conversion coating led to the formation of an Al-Zr-O-F layer, which may contribute to the formation of chemical bonds with PPS during the joining cycle.
- Electrochemical pre-treatments, especially phosphoric acid anodizing, led to a highly porous oxide layer with very small diameter pores. Slight changes in chemical composition were also identified by the addition of phosphorus to the surface.
- Phosphoric acid anodizing + primer specimens had a very compact primer layer, which did not prominently alter the surface roughness. Nevertheless, a very thick carbon-based epoxy primer layer was formed with

whisker-like particles of chromium and strontium oxides as corrosion inhibitors. The carbon-based epoxy layer is also expected to form strong chemical bonds with the PPS during the FSpJ process.

- All surface pre-treatments increased the SLS and CT strength of the joints. PAA-P specimens demonstrated the highest increase in lap-shear strength of 8788 ± 62 N (approximately 10 times higher than the AR condition with 878 ± 89 N) as a result of the formation of the strong carbon-carbon chemical bond. Mechanical, chemical and electrochemical pre-treatments also improved the mechanical strength of the joints. The improvement of the SLS strength was approximately at a similar level for these surface pre-treatments.
- The average strength was approximately 10-30 % in case of the CT specimens compared to the respective SLS joints. Such behavior was related to the shape and angle of the generated asperities on the surface of the aluminum due to the mechanical grinding, sandblasting and phosphoric acid anodizing pre-treatments.
- Fracture surface analysis revealed that failure of SLS joints occurs primarily in the first plies of the composite. Parts of the PPS matrix and carbon fibers were detected on the surface of the aluminum after the failure of the joint. By contrast, with phosphoric acid anodizing + primer surface pre-treated specimens failure took place both in the composite and the primer layer indicating a strong bond between the parts.

Acknowledgements

This work was supported by Helmholtz Association (grant number VH-NG-626). The authors would also like to thank Mr. Fernando Fernandez and Mr. Marcos Miyazaki (Embraer Co., Brazil) for providing parts of the aluminum surface pre-treatments.

References

1. Mallick PK (2010) Joining for lightweight vehicles. In: Mallick PK (ed) Materials, design and manufacturing for lightweight vehicles. Woodhead Publishing Ltd., Cambridge, pp 275-308
2. Grujicica M, Sellappana V, Omara MA, Seyrb N, Obieglob A, Erdmannc M, Holzleitner J (2008) An overview of the polymer-to-metal direct-adhesion hybrid technologies for load-bearing automotive components. J Mater Proc Technol 197 (1-3):363-373
3. S. Katayama, Y. Kawahito (2008) Laser direct joining of metal and plastic. Scripta Materialia 59:1247-1250
4. Mitschang P, Velthuis R, Didi M (2013) Induction Spot Welding of Metal/CFRPC Hybrid Joints. Adv Eng Mater. doi:DOI: 10.1002/adem.201200273
5. Amancio-Filho ST, Bueno C, dos Santos JF, Huber N, Hage Jr. E (2011) On the feasibility of friction spot joining in magnesium/fiber-reinforced polymer composite hybrid structures. Mater Sci Eng A 528:3841-3848. doi:10.1016/j.msea.2011.01.085
6. Amancio-Filho ST, dos Santos JF (2012) Method for joining metal and plastic workpieces.
7. Goushegir SM, dos Santos JF, Amancio-Filho ST (2014) Friction Spot Joining of aluminum AA2024/carbon-fiber reinforced poly(phenylene sulfide) composite single lap joints: Microstructure and mechanical performance. Mater Des 54:196-206
8. Esteves JV, Goushegir SM, dos Santos JF, Canto LB, Hage Jr. E, Amancio-Filho ST (2014) Friction spot joining of aluminum AA6181-T4 and carbon fiber-reinforced poly(phenylene sulfide): Effects of process parameters on the microstructure and mechanical strength. Mater Des 66 (Part B):437-445. doi:10.1016/j.matdes.2014.06.070
9. Goushegir SM, dos Santos JF, Amancio-Filho ST (2015) Influence of process parameters on mechanical performance of AA2024/CF-PPS friction spot joints. Mater Des 83:431-442
10. Goushegir SM, Scharnagl N, dos Santos JF, Amancio Filho ST (2015) XPS analysis of the interface between AA2024-T3/CF-PPS friction spot joints. Surf Interf Anal DOI 10.1002/sia.5816. doi:DOI 10.1002/sia.5816
11. Goushegir SM, dos Santos JF, Amancio Filho ST (2016) Failure and fracture micro-mechanisms in metal-composite single lap joints produced by welding-based joining techniques. Composites: Part A 81:121-128
12. Baldan A (2004) Review Adhesively-bonded joints and repairs in metallic alloys, polymers and composite materials: Adhesives, adhesion theories and surface pretreatment. J Mater Sci 39:1-49
13. Creton C (1997) Materials Science of Pressure-Sensitive Adhesives. In: Meijer HEH (ed) Materials Science and Technology, vol 18. Wiley-VCH Verlag, Weinheim, pp 707-741
14. Gutowski TG (1986) The Mechanics of Composite Deformation During the Manufacturing Process. Paper presented at the First Conference of Composite Materials, Dayton, OH,
15. Molitor P, Young T (2002) Adhesives bonding of a titanium alloy to a glass fibre reinforced composite material. Int J Adhes Adhes 22 (2):101-107

16. Critchlow GW, Yendall KA, Bahrani D, Quinn A, Andrews F (2006) Strategies for the replacement of chromic acid anodising for the structural bonding of aluminium alloys. Int J Adhes Adhes 26:419-453
17. Critchlow GW, Brewis DM (1996) Review of surface pretreatments for aluminium alloys. Int J Adhes Adhes 16:255-275
18. Harris AF, Beevers A (1999) The effects of grit-blasting on surface properties for adhesion. Int J Adhes Adhes 19:445-452
19. Kinloch AJ, Bishop HE, Smart NR (1982) Surface Analysis and Bonding of Aluminium-Magnesium Alloys. The Journal of Adhesion 14 (2):105-118
20. Asgharifar M, Mazar Atabaki M, Kovacevic R (2014) Characterization of the surface topography of arc-treated aluminum alloys by fractal geometry. Manufacturing Letters 2 (2):26-29
21. Chidambaram D, Clayton CR, Halada GP (2006) The role of hexafluorozirconate in the formation of chromate conversion coatings on aluminum alloys. Electrochimica Acta 51:2862-2871
22. J.H. Nordlien, J.C. Walmsley, H. Osterberg, K. Nisancioglu (2002) Formation of a zirconium-titanium based conversion layer on AA 6060 aluminium. Surf Coat Technol 153 (1):72-78
23. N. Fin, H. Dodiuk, A.E. Yaniv, L. Drori (1987) Oxide Treatments of Al 2024 for Adhesive Bonding - Surface Characterization. Appl Surf Sci 28:11-33
24. Yu S, Zhang R, Tang Y, Ma Y, Du W (2013) Composition and Performance of Nanostructured Zirconium Titanium Conversion Coating on Aluminum-Magnesium Alloys. J Nanomaterials 2013
25. S.G. Prolongo, G. del Rosario, A. Urena (2006) Comparative study on the adhesive properties of different epoxy resins. Int J Adhes Adhes 26:125-132
26. Boutar Y, Naïmi S, Mezlini S, Ali MBS (2016) Effect of surface treatment on the shear strength of aluminium adhesive single-lap joints for automotive applications. Int J Adhes Adhes 67:38-43
27. Balle F (2009) Ultraschallschweißen von Metall / C-Faser_Kunststoff (CFK) - Verbunden. PhD thesis, University of Kaiserslautern, Kaiserslautern
28. Dursun T, Soutis C (2014) Recent developments in advanced aircraft aluminium alloys. Mater Des 56:862-871
29. Wakeman MD, Manson JAE (2006) Cost analysis. In: Long AC (ed) Design and Manufacture of Textile Composites. CRC Press,
30. Technical datasheet Corundum, WIWOX GmbH Surface Systems (2009).
31. Alodine 4850 Sicherheitsdatenblatt gemäß Verordnung (EG) Nr. 1907/2006 (2014). Henkel Co
32. ASTM D3163 - 01 (2008) Standard Test Method for Determining Strength of Adhesively Bonded Rigid Plastic Lap-Shear Joints in Shear by Tension Loading. ASTM International
33. DIN EN ISO 14272 (2002) Specimen dimensions and procedure for cross tension testing resistance spot and embossed projection welds. DIN
34. Pocius AV (2012) Adhesion and Adhesives Technology: An Introduction. 3rd edn. Hanser,
35. Ebnesajjad S (ed) (2011) Handbook of Adhesives and Surface Preparation: Technology, Applications and Manufacturing. 1st edn. Elsevier,
36. Hyland MM (2003) Surface Chemistry of Adhesion to Aluminum. In: Totten GE, MacKenzie DS (eds) Handbook of Aluminum: Alloy Production and Materials Manufacturing, vol 2. Marcel Dekker,
37. Wenzel RN (1936) Resistance of solid surfaces to wetting by water. Ind Eng Chem 28 (8):988-994
38. Packham DE (1983) The Adhesion of Polymers to Metals: The Role of Surface Topography. In: Mittal KL (ed) Adhesion Aspects of Polymeric Coatings. Plenum Press, New York, pp 19-44
39. Lunder O, Walmsley JC, Mack P, Nisancioglu K (2005) Formation and characterisation of a chromate conversion coating on AA6060 aluminium. Corr Sci 47:1604-1624
40. Venables JD (1984) Review Adhesion and durability of metal-polymer bonds. J Mater Sci 19:2431-2453
41. Le Coz F, Arurault L, Datas L (2010) Chemical analysis of a single basic cell of porous anodic aluminium oxide templates. Mater Charac 61:283-288
42. Solomon JS, Hanlin DE (1980) AES and SEM Characterization of Anodized Aluminum Alloy Adherends for Adhesive Bonding Application. App Surf Sci 4:307-323
43. Treverton JA, Ball J, Johnson D, Vickerman JC, West RH (1990) SSIMS, XPS and Microstructural Studies of ac-Phosphoric Acid Anodic Films on Aluminium. Surf Interf Anal 15:369-376
44. Digby RP, Packham DE (1995) Pretreatment of aluminium: topography, surface chemistry and adhesive bond durability. Int J Adhes Adhes 15:61-71
45. Hughes AE, MacRae CM, Wilson NC, Tropy A, Muster TH, Glenn AM (2010) Sheet AA2024-T3: A new investigation of microstructure and composition. Surf Interf Anal 42 (4):334-338
46. Gao M, Feng CR, Wei RP (1998) An analytical electron microscopy study of constituent particles in commercial 7075-T6 and 2024-T3 alloys. Metall Mater Trans A 29 (4):1145-1151
47. Boag A, Hughes AE, Wilson NC, Tropy A, MacRae CM, Glenn AM, Muster TH (2009) How complex is the microstructure of AA2024-T3? Corrosion Sci 51 (8):1565-1568
48. Prolongo SG, Urena A (2009) Effect of surface pre-treatment on the adhesive strength of epoxy–aluminium joints. Int J Adhes Adhes 29 (1):23-31

49. Johnsen BB, Lapique F, Bjorgum A, Walmsley J, Tanem BS, Luksepp T (2004) The effect of pre-bond moisture on epoxy-bonded sulphuric acid anodised aluminium. Int J Adhes Adhes 24:183-191
50. Sheasby PG, Pinner R, Wernick S (eds) (2001) The surface treatment and finishing of aluminium and its alloys, Volume 1. ASM International, Materials Park, OH
51. Davis GD, Sun TS, Ahearn JS, Venables JD (1982) Application of surface behaviour diagrams to the study of hydration of phosphoric acid-anodized aluminium. J Mater Sci 17 (6):1807-1818
52. Baer DR, Clayton CR, Davis GD, Halada GP (eds) (2001) State-of-the-art Application of Surface and Interface Analysis Methods to Environmental Material Interactions: In Honor of James E. Castle's 65th Year. The Electrochemical Society, New Jersey
53. Kinloch AJ (1987) Adhesion and Adhesives: Science and Technology. First edn. Springer, Cambridge
54. Bland DJ, Kinloch AJ, Watts JF (2013) The Role of the Surface Pretreatment in the Durability of Aluminium-Alloy Structural Adhesive Joints: Mechanisms of Failure. J Adh 89 (5):369-397
55. Rocher JP, Quenisset JM, Naslain R (1989) Wetting improvement of carbon or silicon carbide by aluminium alloys based on a K2ZrF6 surface treatment: application to composite material casting. J Mater Sci 24 (8):2697-2703
56. Schamm S, Fedou R, Rocher JP, Quenisset JM, Naslain R (1991) The K2ZrF6 wetting process: Effect of surface chemistry on the ability of a SiC-Fiber preform to be impregnated by aluminum. Metall Trans A 22 (9):2133-2139
57. Kinloch AJ, Little MSG, Watts JF (2000) The Role of the Interphase in the Environmental Failure of Adhesive Joints. Acta Materialia 48:4543-4553
58. van der Leeden MC, Frens G (2002) Surface Properties of Plastic Materials in Relation to Their Adhering Performance. Adv Eng Mater 4 (5):280-289
59. Seidlitz H, Ulke-Winter L, Kroll L (2014) New Joining Technology for Optimized Metal/Composite Assemblies. J Eng 2014